IEEE Access
Multidisciplinary | Rapid Review | Open Access Journal

Received 24 June 2022, accepted 12 July 2022, date of publication 21 July 2022, date of current version 27 July 2022.

Digital Object Identifier 10.1109/ACCESS.2022.3192967

RESEARCH ARTICLE

Fuzzy Active Contour Model With Markov Random Field for Change Detection

FEI XIE[1,2], (Member, IEEE), WENYUAN QIAO[1,3], TIANQI GAO[1,3], QUN DUAN[4], TIANSHI LUO[3], AND HAO LI[3], (Member, IEEE)

[1]School of AOAIR, Xidian University, Xi'an 710071, China
[2]School of Computer Science, Northwestern Polytechnical University, Xi'an 710072, China
[3]Key Laboratory of Intelligent Perception and Image Understanding of Ministry of Education of China, School of Electronic Engineering, Xidian University, Xi'an 710071, China
[4]School of Computer Science, Xianyang Normal University, Xianyang, Shaanxi 712000, China

Corresponding author: Wenyuan Qiao (21021110043@stu.xidian.edu.cn)

This work was supported in part by the National Natural Science Foundation of China under Grant 61973249, in part by the Key Research and Development Programs of Shaanxi Province under Grant 2021ZDLGY02-06, in part by the National Defense Science and Technology Key Laboratory Fund under Project 6142101210202, in part by the Natural Science Foundation of Shaanxi, Department of Education under Grant 19JC041, and in part by the Qin Chuangyuan Cited the High-Level Innovative and Entrepreneurial Talent Project under Project 2021QCYRC4-49.

ABSTRACT The traditional active contour models are sensitive to the speckle noise in the synthetic aperture radar (SAR) images. In this paper, the Markov random field (MRF) theory is incorporated into the fuzzy active contour model to detect the changes of multitemporal SAR images. In the proposed method, neighboring information is considered to modify the pointwise prior probability for exploiting the mutual and spatial information. In addition, we incorporate MRF into the fuzzy active contour model and get the resulting MRF-based energy function. Finally, we drive the associated first variation of the energy function to compute the fuzzy membership. Due to the introduction of MRF, the proposed MRF-based fuzzy active contour model is robust to the speckle noise in the SAR images and can achieve accurate change detection results. Experiments on four SAR image datasets demonstrate that the proposed MRF-based fuzzy active contour model is able to accurately segment the difference image and has better performance in comparison with other change detection techniques.

INDEX TERMS Fuzzy active contour model, Markov random field, change detection, synthetic aperture radar.

I. INTRODUCTION

Multitemporal change detection (MTCD) in SAR images captured at different dates over the same geographical location is a significant application in image processing field [1]–[3]. In the past few years, MTCD has attracted widespread interest due to lots of real-world applications in diverse academic disciplines, such as environmental monitoring, damage assessment, agricultural surveys and others [4]–[6]. The goal of MTCD is to generate an accurate change map which represents the changed and unchanged regions.

The associate editor coordinating the review of this manuscript and approving it for publication was Wenming Cao.

In general, a popular way of performing unsupervised MTCD in SAR images consists of two stages [7], [8]. In the first place, a logarithmic or mean ratio operator is used to compare two co-registered remote sensing images acquired at different dates over the same area to generate a so-called ''difference image'' (DI) [9]. Secondly, a certain method is applied to segment the DI and generate a final change map which is a binary image representing the changed and unchanged regions. It can be clearly observed from above that the change detection task here can be formulated as an image segmentation issue. There are lots of methods which have been widely employed in image segmentation task, for instance, thresholding, clustering, edge detection, region extraction [10]–[14]. Many methods

based on these strategies have been proposed for MTCD including Kittler and Illingworth thresholding algorithm (K&I) [11], fuzzy c-means algorithm (FCM) [13], [15], graph-cut algorithm [16] and others [17]–[19]. Among these methods, active contour models (ACMs) perform better with higher accuracy of segmentation [20]–[24] and allow to be easily formulated by minimizing a predefined energy function that incorporates various information of the image.

In light of the discrepancy presented in the ways of forces impelling the evolution, ACMs mainly conclude two categories, edge-based and region-based [25]–[30]. Caselles *et al.* proposed the geodesic ACM [31], which is one of the most widely applied and classical ACM using edge-based information through the level set method. For boundary detection, a special and novel instance of the active contours or energy-snakes approach is shown in this model, which guides to generate a geodesic curve derived from the image content in a fixed Riemannian space. However, these edge-based ACMs could not find the correct boundaries of the object when the images are filled with noise. For MTCD in SAR images, as the edges of object regions in a difference image are usually blurred, it is difficult for the edge-based ACMs to capture the edges accurately.

To avoid suffering the disadvantage of the edge-based ACMs, some region-based ACMs guiding the contour to the object boundary by making use of the global intensity information of the image have been proposed. Region-based ACMs for segmentation are proposed and the primary idea is to evolve the curve to the object boundary with the global statistical information of the image, such that they can overcome the shortcoming of the edge-based ACMs. In these models which are based on the Mumford-Shah segmentation model [32], images are partitioned into several smooth regions with short boundaries in piece-wise. For example, Chan and Vese (CV) has proposed an outstanding model which is known as active contour without edges [33]. This region-based ACM, which is the classical and widely used, can detect contour without gradient information. Benifiting from the approach, the optimization becomes easier and can cope with the topology changes of segmentation naturally. In order to assure the accuracy of segmentation and the stability of evolution in CV model, the level set function (LSF) is necessary to be maintained in a suitable condition. It means that the LSF cannot be too sharp or too flat in a neighborhood around the zero level set. Usually, the procedure re-initialization [34] is periodically applied to prevent the LSF from typically developing irregularities and reshape the degraded LSF as a signed distance function (SDF) in the course of evolution. But the introduction of the re-initialization not only results in the conundrum of when and how to launch the procedure [35] but gives rise to a large amount of computation and non-negligible numerical errors.

Moreover, statistical approaches attract researchers' attention for ACMs based segmentation. Zhu and Yuille proposed region competition model (RC) [36] based on Bayes and Minimum Description Length (MDL) criterion. Then Cremers *et al.* reviewed the statistical active contour models (SAC) [37] for level set segmentation. In order to reject local minima, fuzzy systems have been incorporated into the traditional ACMs [38]–[41]. To make the model more robust, Krinidis and Chatzis has been inspired by the FCM algorithm and proposed the fuzzy energy-based active contour model (FEBAC) [40], in which the object-oriented membership of each pixel in the image is defined with fuzzy logic. It has been demonstrated that the resulting fuzzy energy is capable of keeping away from local minima, which is a characteristic of fuzzy ACMs [42]–[45].

With the view of relieving the effects of speckle noise in the task of MTCD [46], neighboring information is considered in most of change detection algorithms [13], [47]. In this paper, we take Markov Random Field (MRF) [48]–[51] into consideration to improve the region-based active contour models. MRF models have been widely employed in varieties of tasks in image processing field, such as semantic segmentation, image restoration, edge detection and others [52]–[54], because those models introduce the mutual influences among the pixels in the image. Chatzis and Varvarigou proposed a KL divergence based fuzzy objective, which estimates the MRF prior [48] with a mean-field-like approximation. To modify the membership of each pixel, an additional term was added in the MRF energy function [55]. The resulting MRF-based fuzzy c-means algorithm (FCMA) was used to detect the changes of multitemporal SAR images.

In this paper, we propose an MRF-based fuzzy active contour (MRFFAC) model for change detection of SAR images. First of all, we compare several energy functions of region-based ACMs with some clustering techniques. Then, a novel fuzzy ACM based on the MRF theory is proposed, which is applied to detect the changed regions of SAR image time-series. In the proposed approach, the pointwise prior probability is modified to employ mutual and spatial information. Then the MRF-based energy function is proposed and its first variation of it is derived to formulate the updating formula.

The contribution of this paper includes the following three aspects: (1) A modified pointwise prior probability is proposed to consider the mutual and spatial information, which has the ability to measure the margin locating between the changed class and unchanged class accurately. (2) The MRF theory is successfully incorporated into the fuzzy ACM and the associated updating formula is derived. The resulting model is less sensitive to the speckle noise existing in the SAR images and achieves superior performance for MTCD. (3) We substantiate the superiority of MRFFAC on the four SAR image change detection datasets. The organization of the rest of this paper is as follows: a brief comparison between several ACMs and unsupervised clustering techniques is provided in Section 2. Secondly, Section 3 introduces the proposed approach in details. Then, Section 4 describes the experimental study. Finally, concluding remarks are given in Section 5.

II. BACKGROUND

The energy functions of region-based ACMs are very similar to some traditional clustering algorithms, for example, k-means algorithm, FCMA and so on. The comparisons between ACMs and clustering algorithms will be described in this section and these algorithms are also used as the competing methods in the experiments.

A. k-MEANS ALGORITHM AND CV MODEL

Among the hard clustering approaches, the k-means algorithm has been mostly applied to image segmentation. Its energy function is described as:

$$E = \sum_{i=1}^{N}\sum_{k=1}^{c} \|x_i - v_k\|^2 \tag{1}$$

where N denotes the total number of pixels in the image I, c represents the number of clusters with a range from 2 to N, x_i is the i-th pixel in the image I, $\|\cdot\|$ is the Euclidean norm and v_k stands for the cluster centers or prototypes of the clusters.

In CV model, image segmentation can be considered as seeking out an optimal contour C through the energy function written as follows:

$$E_{CV}(C) = \int_{inside(C)} |I(u,v) - c_1|^2 dudv + \int_{outside(C)} |I(u,v) - c_2|^2 dudv \tag{2}$$

where c_1 and c_2 are both constants which depend on C and denotes the averages of the image regions respectively inside and outside of the curve C.

Obviously, for $k = 2$, the energy function of k-means algorithm (Eq. (1)) is very similar to CV model (Eq. (2)). In order to minimize the energy function above (Eq. (2)), the level set method is considered to be a suitable solution. In detail, with the help of the zero level set of a Lipschitz function $\phi : \Omega \to R$, the curve C can be indicated in a definite form, such that

$$\begin{cases} ccinside(C) = \{(u,v) \in \Omega : \phi(u,v) > 0\} \\ outside(C) = \{(u,v) \in \Omega : \phi(u,v) < 0\} \\ C = \{(u,v) \in \Omega : \phi(u,v) = 0\} \end{cases} \tag{3}$$

Then the energy function $E_{CV}(C)$ described in the above can be written as:

$$E_{CV}(\phi) = \int_{\Omega} H(\phi(u,v))|I(u,v) - c_1|^2 dudv + \int_{\Omega} (1 - H(\phi(u,v)))|I(u,v) - c_2|^2 dudv \tag{4}$$

where $H(\cdot)$ is Heaviside function.

B. FUZZY C-MEANS ALGORITHM AND FEBAC MODEL

As an iterative clustering method, the FCMA minimizes the weighted sum of squared error within group, and its objective function E_m is described as follows:

$$E_m = \sum_{i=1}^{N}\sum_{k=1}^{c} \left[\zeta_{ki}^m \|x_i - v_k\|^2\right] \tag{5}$$

where ζ_{ki} represents the degree of membership that the pixel x_i of the image belongs to the k-th cluster, m is a weighting exponent, ranging from 1 to ∞.

Then, the objective function E_m shown in Eq. (5) can be minimized by updating the cluster center v_k and degree of the membership ζ_{ki} orderly as follows:

$$v_k = \frac{\sum_{i=1}^{N} u_{ki}^m x_i}{\sum_{i=1}^{N} u_{ki}^m} \tag{6}$$

$$\zeta_{ki} = \frac{1}{\sum_{j=1}^{c} \left(\frac{\|x_i - v_k\|^2}{\|x_i - v_j\|^2}\right)^{\frac{1}{m-1}}} \tag{7}$$

Algorithm 1 Algorithm of FEBAC.

1: **Input:** The image I.
2: **Ouput:** The segmentation result.
3: **Initialization:** Initialize a partition for the image.
4: Set the threshold for the degree of membership ζ at 0.5.
5: **while** *not converged* **do**
6: Compute v_1 and v_2 by
7:

$$v_1 = \frac{\int_{\Omega}[\zeta(u,v)]^m I(u,v) dudv}{\int_{\Omega}[\zeta(u,v)]^m dudv} \tag{8}$$

8:

$$v_2 = \frac{\int_{\Omega}[1 - \zeta(u,v)]^m I(x,y) dudv}{\int_{\Omega}[1 - \zeta(u,v)]^m dudv} \tag{9}$$

9: Calculate the new degree of membership by
10:

$$\zeta_{ki}(u,v) = \frac{1}{1 + \left(\frac{\lambda_1 (I(u,v) - v_1)^2}{\lambda_2 (I(u,v) - v_2)^2}\right)^{\frac{1}{m-1}}} \tag{10}$$

11: Compute $\triangle F$, which represents the difference of the energy obtained between the current and the last iterations.
12: **end while**
13: Return the segmentation result.

The FEBAC model defines a pseudo level set, which can be formulated similarly to Eq. (3) as follows:

$$\begin{cases} ccinside(C) = \{(u,v) \in \Omega : \zeta(u,v) > 0.5\} \\ outside(C) = \{(u,v) \in \Omega : \zeta(u,v) < 0.5\} \\ C = \{(u,v) \in \Omega : \zeta(u,v) = 0 \quad \} \end{cases} \tag{11}$$

Inspired by Eq. (4), the FEBAC model adds fuzzy logic into CV model by replacing $H(\phi)$ with ζ. The energy function of FEBAC is performed as follows:

$$E(u) = \int_{\Omega} \zeta(u,v)^m |I(u,v) - c_1|^2 dudv + \int_{\Omega} (1-\zeta(u,v))^m |I(u,v) - c_2|^2 dudv \quad (12)$$

The pseudo code of FEBAC is shown in **Algorithm 1**. In the FEBAC model, a balanced and novel technique, which has a unique ability to refuse the weak local minima through figuring out the fuzzy energy alterations directly, is provided. However, as shown in **Algorithm 1**, it updates the membership ζ and the center c by Eq. (7) and Eq. (6), which is very similar to the framework of FCM.

III. METHODOLOGY

As mentioned above, the generation and the analysis of DI compose the main process of change detection. Considering two SAR images having been coregistered $I_A = \{I_A(u,v), 1 < u < H, 1 < v < W\}$ and $I_B = \{I_B(u,v), 1 < u < H, 1 < v < W\}$, either of which is of size $H \times W$, both are captured by a SAR sensor respectively at t_1 and t_2. Then, DI is generated through applying the log-ratio operator and denoted as $I_{LR} = \{I_{LR}(u,v), 1 < u < H, 1 < v < W\}$. The next task is to analyze the DI. Motivated by the above descriptions, we design a novel fuzzy ACM based on Markov Random Field to reduce the effect of the speckle noise. First, the novel energy function of MRF is introduced. Next, In this Section, we'll detailedly discribe the proposed algorithm, which is termed as MRFFAC for short.

A. MODIFICATION ON THE ENERGY FUNCTION OF THE MRF

For MTCD in SAR images, the identification of changed regions is implemented by segmenting DI into the changed class and unchanged class. We use the membership matrix $\{\phi_k | k = \{c_+, c_-\}\}$ to represent the degree of the membership of the image I in the k class. To avoid confusion, we define the membership ϕ as:

$$\begin{cases} \phi_{c_+} = \phi \\ \phi_{c_-} = 1 - \phi \end{cases} \quad (13)$$

where u is the unchanged class and c is the changed class.

On the basis of the values of the membership matrix $\{\phi\}$ and hard division with the threshold 0.5, we use u and c to mark unchanged and changed pixels, respectively. Then we obtain two sets $\{\Phi_k | k = \{c_+, c_-\}\}$:

$$\{\Phi_k | k = \{c_+, c_-\}\} = \begin{cases} \{\Phi_{c_+}\} = \{\phi | \phi \geq 0.5\} \\ \{\Phi_{c_-}\} = \{1 - \phi | \phi < 0.5\} \end{cases} \quad (14)$$

As described in the above, it's necessary to find a robust energy function that takes full advantage of the relationship among neighbors. In an effort to propose an adequate energy function, we design a convenient and the simplest approach, getting the mean of the degree of the membership of the entire neighbors, through which the pointwise prior probability is of high accuracy. And the energy function can be described as:

$$E_{ki} = -\ln(P_{ki}), k = \{c_+, c_-\} \quad (15)$$

where

$$P_{ki} = \underset{j \in N, j \neq i}{mean} \left(\phi_{kij} | \phi_{kij} \in \{\Phi_k\}\right) \quad (16)$$

i is the index of the central pixel, and N is the neighborhood system of the i-th pixel.

It can be derived from Eq. (16) that only the membership of pixels which belongs to the same category as that of the central one is utilized. The error engendered by the other pixels will be reduced through adding the information gained from classification. Whereas, two main drawbacks still exist. First, the margin between the two classes is reduced by utilizing the mean of the membership belonging to the same class. Second, although using the mean of the membership belonging to the same class, we have not considered the membership belonging to the other class. In short, this method is still sensitive to speckle noise because of the narrow margin between the two classes and the absence of the information of the other class.

In order to overcome such defects, we use mutual and spatial information to represent the pointwise prior probability. The degree of attenuation of the neighbors is measured with the Euclidean distance from the central pixel of the class. The summation of the memberships in the neighborhood system with spatial distance can be calculated by

$$s_{ki} = \sum_{j \in N, j \neq i} \frac{1}{d_{ij} + 1} \left(\phi_{kij} | \phi_{kij} \in \{\Phi_k\}\right) \quad (17)$$

where d_{ij} is the distance of the ith central pixel and its jth neighborhood pixel.

So the modified pointwise prior probability can be considered as:

$$P_{ki} = \frac{D_{ki} - \min(\mathbf{D_k})}{\max(\mathbf{D_k}) - \min(\mathbf{D_k})} \quad (18)$$

where $\mathbf{D_k} = \{D_{ki} | D_{ki} = s_{ki} - s_{(\{c_+, c_-\} - k)i}\}$, $\min(\mathbf{D_k})$ and $\max(\mathbf{D_k})$ denote respectively the minimal and the maximal value of the matrix $\mathbf{D_k}$ in the k-th class.

As an example, Fig. 1 shows an example to illustrate the proposed strategy. As shown in Eq. (17) and Eq. (18), the memberships of the pixels belonging to the two classes are utilized. As a consequence of adding the mutual and spatial information into the energy function, the margin between the two classes is assigned by an appropriate way.

B. MRF-BASED FUZZY ACTIVE CONTOUR MODEL

For MTCD in SAR image series, the DI is partitioned into changed region and unchanged region by a fuzzy ACM, and then changes are identified. After the evolving curve

U1	U2	U3
C4	A	U4
C3	C2	C1

(a)

0. 414	0. 5	0. 414
0. 5	A	0. 5
0. 414	0. 5	0. 414

(b)

FIGURE 1. Membership values and damping extent both displayed in 3 × 3 window. (a) Membership Values (ϕ). (b) The degree of attenuation of the neighboring pixels. If the central pixel A is labeled by U, and then D_{UA} can be calculated by $D_{UA} = (0.414U1 + 0.5U2 + 0.414U3 + 0.5U4) - (0.414(1 - C1) + 0.5(1 - C2) + 0.414(1 - C3) + 0.5(1 - C4))$.

C defined in the image domain Ω, a pseudo level set is formulated through ultilizing the membership values ϕ and the hard division mentioned. We define the pseudo level set as follows:

$$\begin{cases} inside(C) = \{z \in I : \phi > 0.5\} \\ outside(C) = \{z \in I : \phi < 0.5\} \\ C = \{z \in I : \phi = 0.5\} \end{cases} \tag{19}$$

The distribution characteristic of the log-ratio SAR image is close to a normal distribution, and it has been explained in [11] and [46]. Considering the intensities of each region obeying a normal distribution, the conditional probability $\{p_{ki}\}$ is given by:

$$p_{ki}(z_i|\mu_k, \sigma_k^2) = \frac{1}{\sqrt{2\pi\sigma_k^2}} \exp\left(-\frac{(z_i - \mu_k)^2}{2\sigma_k^2}\right) \tag{20}$$

where $k = \{c_+, c_-\}$.

The optimal estimate for the mean μ_k can be obtained by:

$$\begin{cases} \mu_{c_+} = \dfrac{\sum\limits_{i=1}^{N} \phi_i z_i}{\sum\limits_{i=1}^{N} \phi_i} \\ \mu_{c_-} = \dfrac{\sum\limits_{i=1}^{N} (1-\phi_i) z_i}{\sum\limits_{i=1}^{N} (1-\phi_i)} \end{cases} \tag{21}$$

and the variance σ_k can be computed by:

$$\begin{cases} \sigma_{c_+}^2 = \dfrac{\sum\limits_{i=1}^{N} \phi_i (z_i - \mu_{c_+})^2}{\sum\limits_{i=1}^{N} \phi_i} \\ \sigma_{c_-}^2 = \dfrac{\sum\limits_{i=1}^{N} (1-\phi_i)(z_i - \mu_{c_-})^2}{\sum\limits_{i=1}^{N} (1-\phi_i)} \end{cases} \tag{22}$$

Then generate the distance matrix $\{d_k\}$

$$d_k = -ln\left[p_{ki}(z_i|\mu_k, \sigma_k^2)\right] \tag{23}$$

Finally, we get the following energy function:

$$E(\phi) = \int_{\Omega} \exp\left(d_{c_+}\right)\phi - \int_{\Omega} \exp\left(d_{c_-}\right)(1 - \phi) \tag{24}$$

And it is minimized through alternating a gradient descent method for the embedding function ϕ. The first variation (also called Gateaux derivative) of the function E is written as:

$$\frac{\partial \phi}{\partial t} = -\frac{\partial E}{\partial \phi} = -\exp\left(d_{c_+}\right)\phi - \exp\left(d_{c_-}\right)(1 - \phi) \tag{25}$$

C. MRFFAC FOR CHANGE DETECTION

It is note that the relationship between intensity I of the SAR image and the underlying backscattering coefficient X is established through a multiplicative model:

$$I = RX \tag{26}$$

where R denotes the normalized random variable of the fading speckle noise. The difference image is acquired by employing a ratio operator to the two SAR images pixel-by-pixel. Then, the log-ratio difference image can be generated by the equation as following:

$$I_{LR} = \left|\log \frac{I_B}{I_A}\right| = \left|\log \frac{R_B}{R_A} + \log \frac{X_B}{X_A}\right| \tag{27}$$

where I_A and I_B are the two SAR images, respectively. As shown in Eq. (27), the original multiplicative speckle noise is ingeniously converted to an additive one.

Algorithm 2 Algorithm of MRFFAC for MTCD in SAR Images.

1: **Input:** The two image I_A and I_B.
2: **Output:** A binary change map.
3: **Generate DI:**
4: Through employing the log-ratio operator, generate the DI by Eq. (27).
5: **Initialization:** The membership matrix $\left\{\phi_i^1\right\}$ is initialized by using the original FCM algorithm and normalize the difference image to [0,1].
6: Set r=1.
7: **while** *not converged* **do**
8: Establish the energy matrix E_{ki}^r.
9: Acquire the pointwise prior probability matrix π_{ki}^r by Eq. (28).
10: Compute the fuzzy membership by Eq. (29).
11: Normalize ϕ by Eq. (30).
12: $r = r + 1$.
13: **end while**
14: Return the binary change map.

The proposed method shown in **Algorithm 2** is composed of the following procedures. In the first place of the iteration, the membership matrix $\left\{\phi_i^1\right\}$ is initialized with the FCM algorithm and the image I is normalized to [0,1]. In the rth iteration, the energy matrix E_{ki}^r is established. Ultilizing Gibbs expression, we calculate the pixelwise prior probability of the MRF, then acquire the pixelwise prior probability matrix π_{ki}^r in the r-th iteration:

$$\pi_{ki}^r = \frac{\exp\left(-E_{ki}^r\right)}{\exp\left(-E_{c_+i}^r\right) + \exp\left(-E_{c_-i}^r\right)} \tag{28}$$

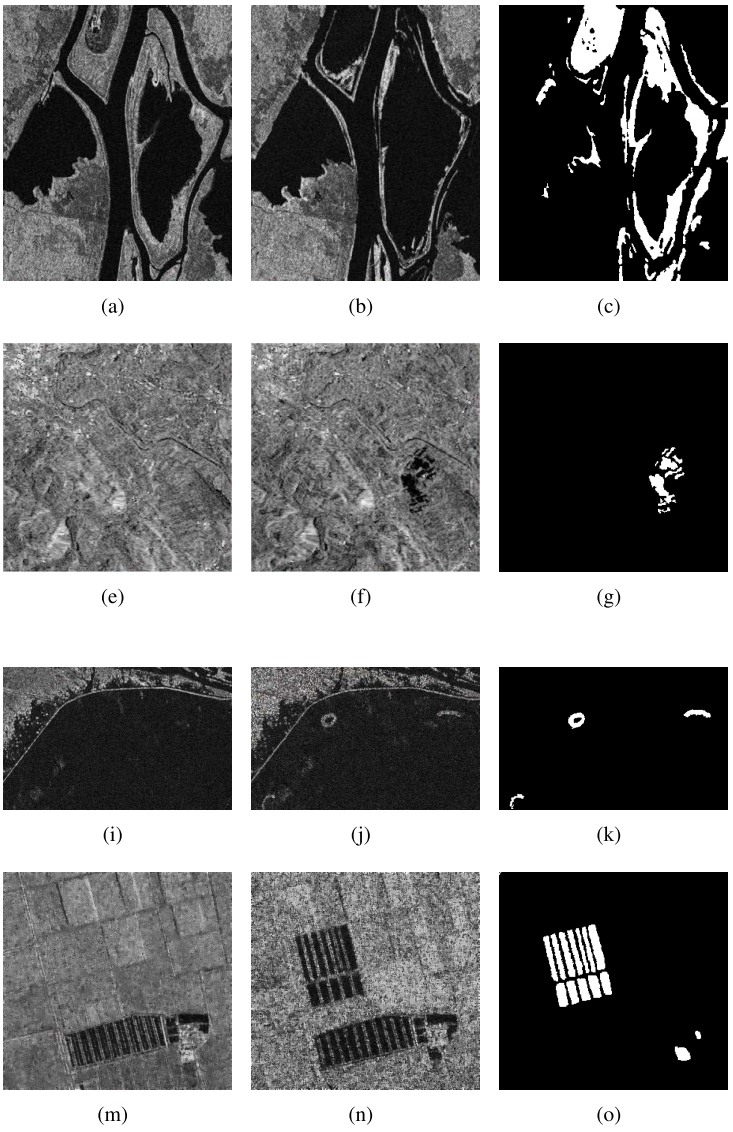

The Fist dataset	
Size	290×350 pixels
Location	The city of Ottawa
Image (a)	May 1997
Image (b)	August 1997
Sensor	RADARSAT SAR sensor

The Second dataset	
Size	301×301 pixels
Location	The city of Bern
Image (a)	April 1999
Image (b)	May 1999
Sensor	European Remote Sensing 2 satellite SAR sensor

The Third dataset	
Size	450×280 pixels
Location	Coastline area of the Yellow River
Image (a)	June 2008
Image (b)	June 2009
Sensor	RADARSAT-2 sensor

The Fourth dataset	
Size	306×291 pixels
Location	Farmland area of the Yellow River
Image (a)	June 2008
Image (b)	June 2009
Sensor	RADARSAT-2 sensor

FIGURE 2. Four datasets used in the experiments. The first column (a, e, i and m) and second column (b, f, j and n) exhibit the SAR images acquired at different dates. The ground truth maps are shown in the third column (c, g, k and o). The fourth column (d, h, l and p) gives the description of these datasets.

In the r-th iteration, we compute the fuzzy membership by Eq. (29)

$$\begin{aligned}\phi^{r+1} = \phi^r + \Delta t\{&-\exp(-d_{c_+})\phi^r \\ &-\exp(-d_{c_-})(1-\phi)^r\}\end{aligned} \tag{29}$$

where $\phi^r = \pi_{c_+}, (1-\phi)^r = \pi_{c_-}$.

Then we normalize ϕ by Eq. (30):

$$\phi = \begin{cases} 0, & if\ \phi \le 0 \\ \phi, & if\ 0 < \phi < 1 \\ 1, & if\ \phi \ge 1 \end{cases} \tag{30}$$

Finally, checking the stability of the solution, if the stop condition is satisfied, we put an end to the algorithm and output a change map.

IV. EXPERIMENTAL STUDIES

For the purpose of validating the effectiveness of the approach proposed above, experiments for CD on four SAR image datasets will be performed in this section. We use ratio method to generate difference images. Finally, the DIs are partitioned into changed class and unchanged class and the region where changes are identified.

A. DATASETS AND QUANTITATIVE MEASURES

The first dataset includes two SAR images (Fig. 2(a) and (b)), either of which is of size 290 × 350 and acquired by RADARSAT SAR sensor over Ottawa. The second one is also composed of two SAR images (Fig. 2(e) and (f), both with the size of 301×301), captured by the European Remote Sensing 2 satellite SAR sensor over a suburb of Bern, Switzerland, and the dates are respectively

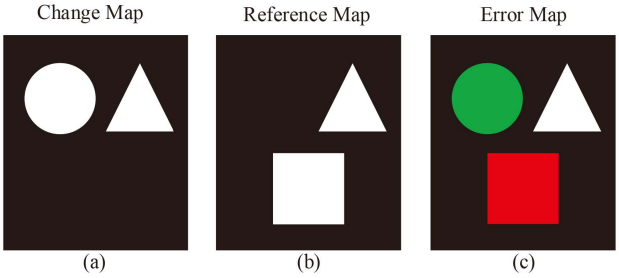

FIGURE 3. Illustration of the missed alarms, false alarms and Kappa statistic: (a) is the change map obtained by a certain algorithm, (b) represents the reference map, and (c) is the error map.

April and May 1999. The last two datasets are derived from two SAR images, with the size of 7666 × 7692, acquired by Radarsat-2 sensor over the district of Yellow River Estuary, China, respectively in June 2008 and June 2009. On account of the unduly huge size of the two images, the detail information is difficult to be shown in one page. So two repressive areas, which are respectively of size 450 × 280 pixels ((Fig. 2(i) and (j))) and 306 × 291 pixels ((Fig. 2(m) and (n)), are selected to construct two datasets.

The quantitative analysis of the experimental results involves four metrics. Fig. 3 shows the illustration of the missed alarms, false alarms and Kappa statistic. Missed alarms (MA) is denoted as the rectangle filled with red in Fig. 3, and it means the number of unchanged pixels that miss being classified when compared to the ground truth. False alarms (FA) is denoted as the circle filled with green in Fig. 3, and it means that the number of unchanged pixels which are in the reference map but classified as the changed class in the change map. Kappa statistic, as a measure of accuracy, takes both commission errors and omission errors into account. And the higher Kappa means the better result of CD. For accuracy assessment, total error (TE) is considered in the experiments. TE represents the total number of classification errors which are caused by either missed alarms or false alarms. Namely, it is the total number of the occurrences of missed alarms and false alarms.

B. EXPERIMENTAL RESULTS

Aiming at verifying the performance of the change CD method designed in this paper, we considered four real multi-temporal SAR datasets and made a comparison with the result acquired through the proposed approach with those results of the k-means algorithm, the FCM algorithm, the fuzzy local information c-means algorithm (FLICM) [47], the improved Chan-Vese algorithm (ICV) [56], the fuzzy energy-based contour model (FEBAC) [40], and expectation-maximization-based level set method (EMLS) [22]. The k-means algorithm, the FCM algorithm, the CV model, and the FEBAC model have been described in Section II. Comparing with the proposed method, which has been employed to SAR images CD in [13], the progressive FLICM [47] is selected here. In the difference image,

TABLE 1. Comparison of CD results about the Ottawa dataset obtained through the seven algorithms.

Algorithm	FA	MA	TE	Kappa
k-means	2173	2704	4877	0.8171
FCM	2173	2704	4877	0.8171
FLICM	222	2587	2809	0.8894
ICV	1842	2305	4147	0.8447
FEBAC	18080	957	19037	0.5085
EMLS	223	7294	7517	0.6612
MRFFAC	382	2253	2635	0.8976

the EMLS method respectively estimates the mean values of pixels changed and unchanged through expectation-maximization, and then improve the accuracy by adding two new energy terms into the level set. In the experiments, we first exhibit the binary change maps acquired by different CD methods. Furthermore, the miss alarms are marked by red and the false alarms are marked by green. Therefore a color image is associated with the binary map in the experiments. Finally, we report the change detection results with metrics in the tables.

1) RESULT ON THE OTTAWA DATASET

In this experiment, the dataset is composed of two SAR images (Fig. 2(a) and (b)), captured over the city of Ottawa. Fig. 4 shows the experimental results acquired by the seven MTCD methods. It is obviously seen that the change maps obtained by FEBAC contain lots of noise. Since lots of red pixels exist in Fig. 4(l), the EMLS method missed detecting many changed regions. It can be found that the change maps obtained by FCM, FLICM, ICV, and the proposed MRFFAC are close to the reference map shown in Fig. 4(o). Furthermore, although the proposed MRFFAC model is able to obtain satisfactory results, some changed regions are not detected in the upper left corner of Fig. 4(m) and (n).

The CD results about the Ottawa dataset are reported in Table 1. The total errors of FEBAC are larger than 19,000 since many regions unchanged are detected as the changed ones. It is demonstrated that the FEBAC mode is sensitive to noise to deal with the Ottawa dataset. As described in Table 1, the total errors of the MRFFAC are a little less than that of FLICM. The value of Kappa of the MRFFAC is larger than the FLICM algorithm. In general, the effectiveness of the proposed algorithm has been verified.

2) RESULT ON THE BERN DATASET

The dataset in this part is a section of two SAR images over Bern, both comprised of 301 × 301 pixels. The change maps acquired by the seven MTCD methods are shown in Fig. 5. Obviously, many unchanged regions are identified as changed ones, on account of noise which is strewn across change maps obtained by the ICV and FEBAC models. To some extent, the change maps generated by other five approaches are similar to the ground truth map in Fig. 5(o). However, the background of change map acquired by the MRFFAC is relatively clear.

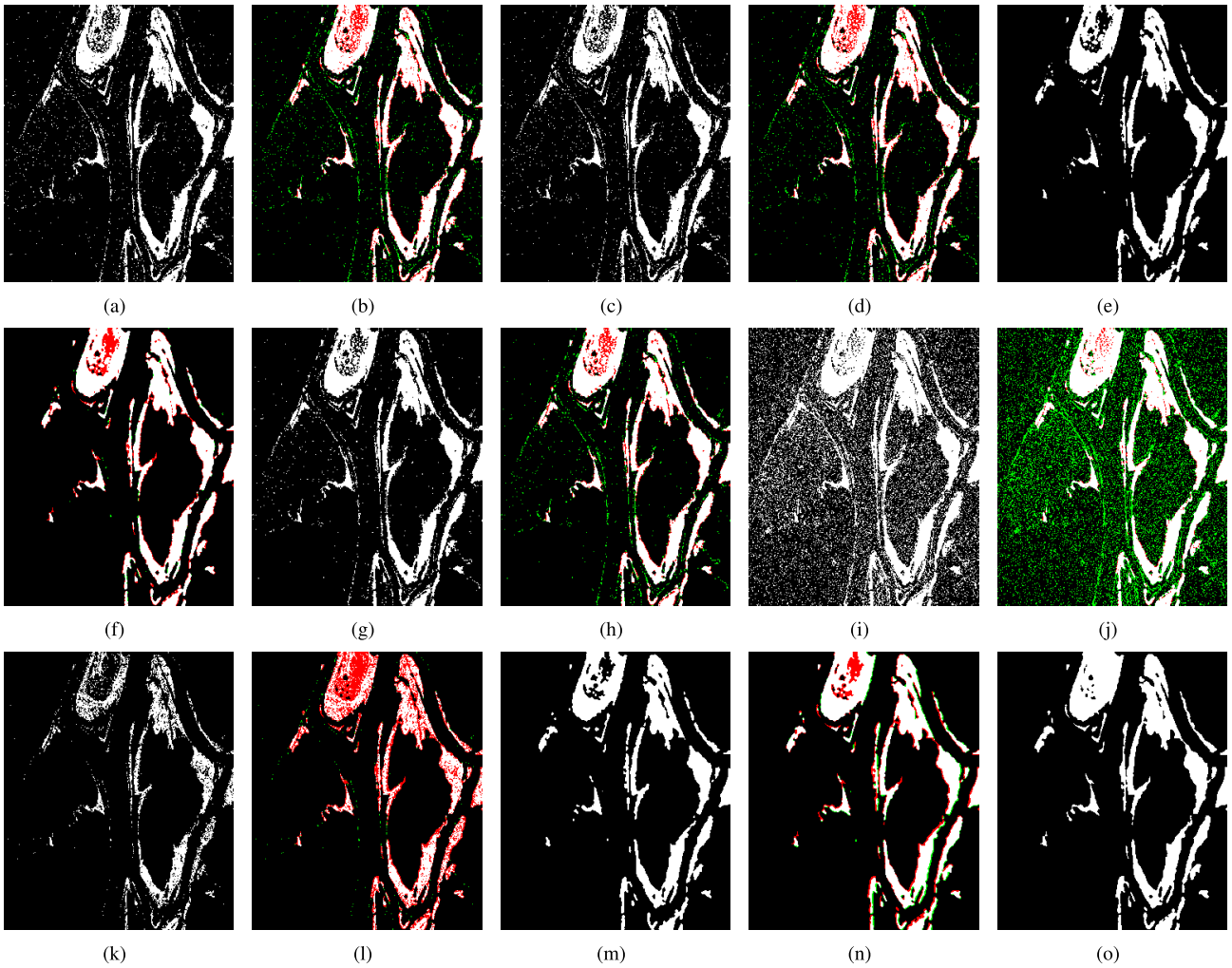

FIGURE 4. Results for the Ottawa dataset obtained by (a) and (b): *k*-means, (c) and (d): FCM, (e) and (f): FLICM, (g) and (h): ICV, (i) and (j): FEBAC, (k) and (l): EMLS, (m) and (n): proposed MRFFAC, and (o): reference image.

TABLE 2. Comparison of CD results on the Bern dataset obtained through the seven algorithms.

Algorithm	FA	MA	TE	Kappa
k-means	361	326	687	0.7032
FCM	422	298	720	0.7002
FLICM	67	236	303	0.8568
ICV	4550	41	4591	0.3122
FEBAC	30289	26	30315	0.0459
EMLS	430	266	696	0.7148
MRFFAC	101	177	284	0.8716

The CD results obtained by the seven MTCD method on the Bern dataset are shown in Table 2. As described in Table 2, the total errors of FEBAC and ICV are larger than 30,000 and 4,500, respectively. The total errors of the other five methods are less than 1,000. Table 2 show that the proposed MRFFAC obtains almost the same results as FLICM. The Kappa yielded by FLICM and MRFFAC are equal to 0.8568 and 0.8716, respectively. The proposed MRFFAC outperforms FLICM obviously. To sum up, the proposed MRFFAC is applicable to the most situations, no matter the changed area is scattered (the Ottawa dataset) or centralized (the Bern dataset).

3) RESULT ON THE COASTLINE AREA OF THE YELLOW RIVER DATASET

A section (450×280 pixels) of two SAR images, obtained by scanning over the local area of Yellow River, are investigated in this experiment. Fig. 6 displays the changes maps, which were acquired by the seven MTCD algorithms. It can be clearly found that most of the CD methods aren't successful detecting changed regions since the two considered SAR images consist of too much speckle noise. As shown in Fig. 6, change maps obtained by FLICM, EMLS and the proposed MRFFAC have very few green pixels. However, some changed regions miss being detected by the EMLS method.

The CD results with four metrics on the Coastline area of the Yellow River dataset are shown in Table 3. As stated in Table 3, the total errors obtained by *k*-means, FCM, ICV, and

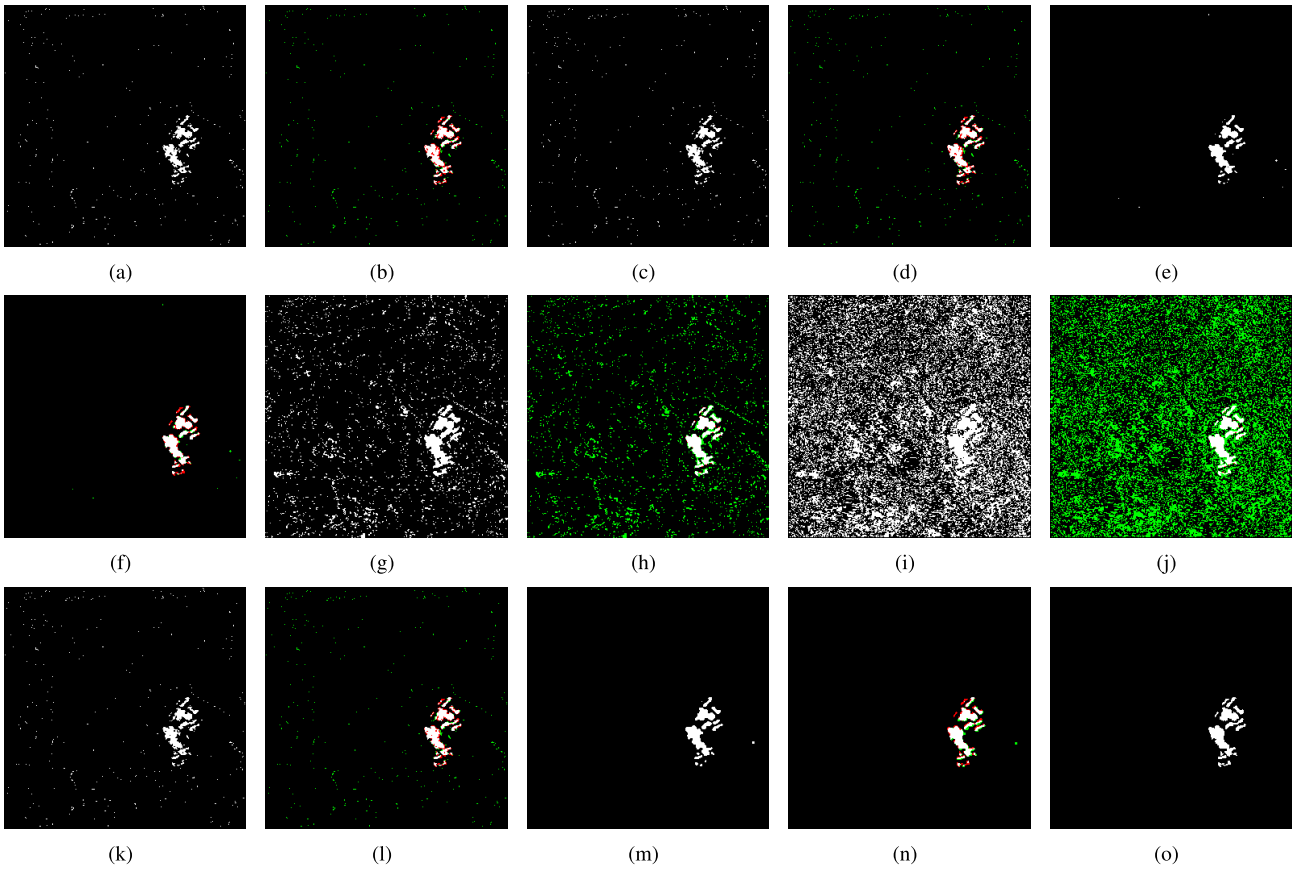

FIGURE 5. Change detection results for the Bern dataset obtained by (a) and (b): *k*-means, (c) and (d): FCM, (e) and (f): FLICM, (g) and (h): ICV, (i) and (j): FEBAC, (k) and (l): EMLS, (m) and (n): proposed MRFFAC, and (o): reference image.

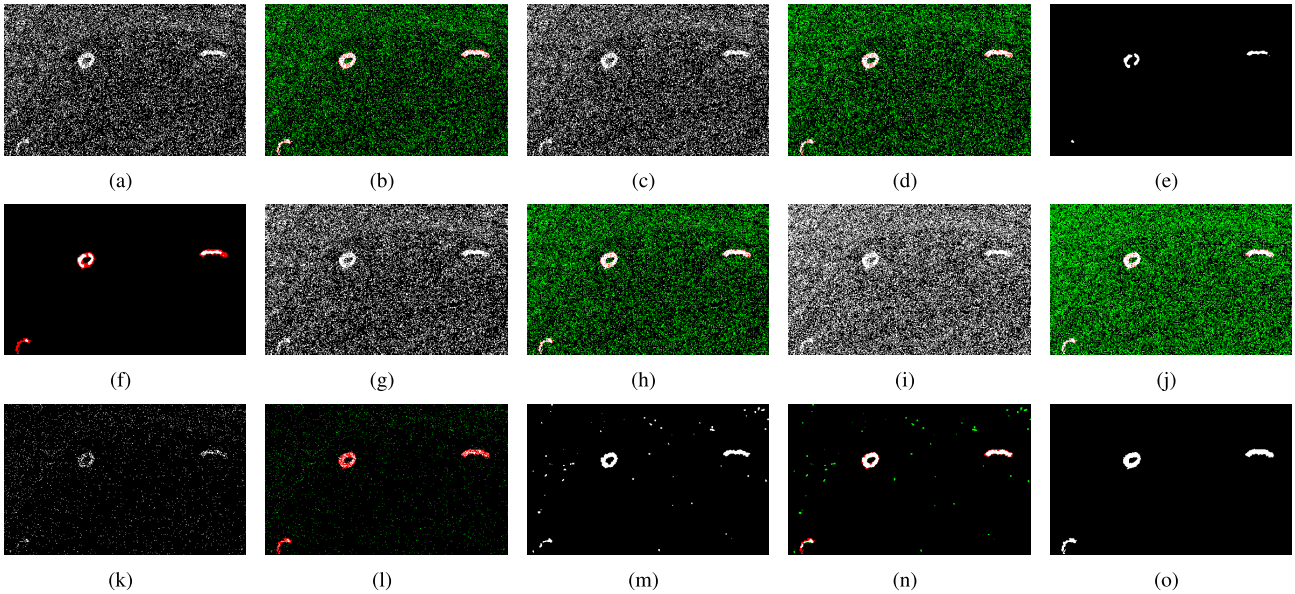

FIGURE 6. Change detection results for the Coastline area of the Yellow River dataset obtained by (a) and (b): *k*-means, (c) and (d): FCM, (e) and (f): FLICM, (g) and (h): ICV, (i) and (j): FEBAC, (k) and (l): EMLS, (m) and (n): proposed MRFFAC, and (o): reference image.

FEBAC are larger than 28,000. The FA value of EMLS is 2593, which is larger than those of FLICM and MRFFAC. Table 3 shows that the proposed MRFFAC and FLICM obtain almost the similar total errors. It can be easily found that the proposed MRFFAC is better than the FLICM due to its conspicuously high values of Kappa.

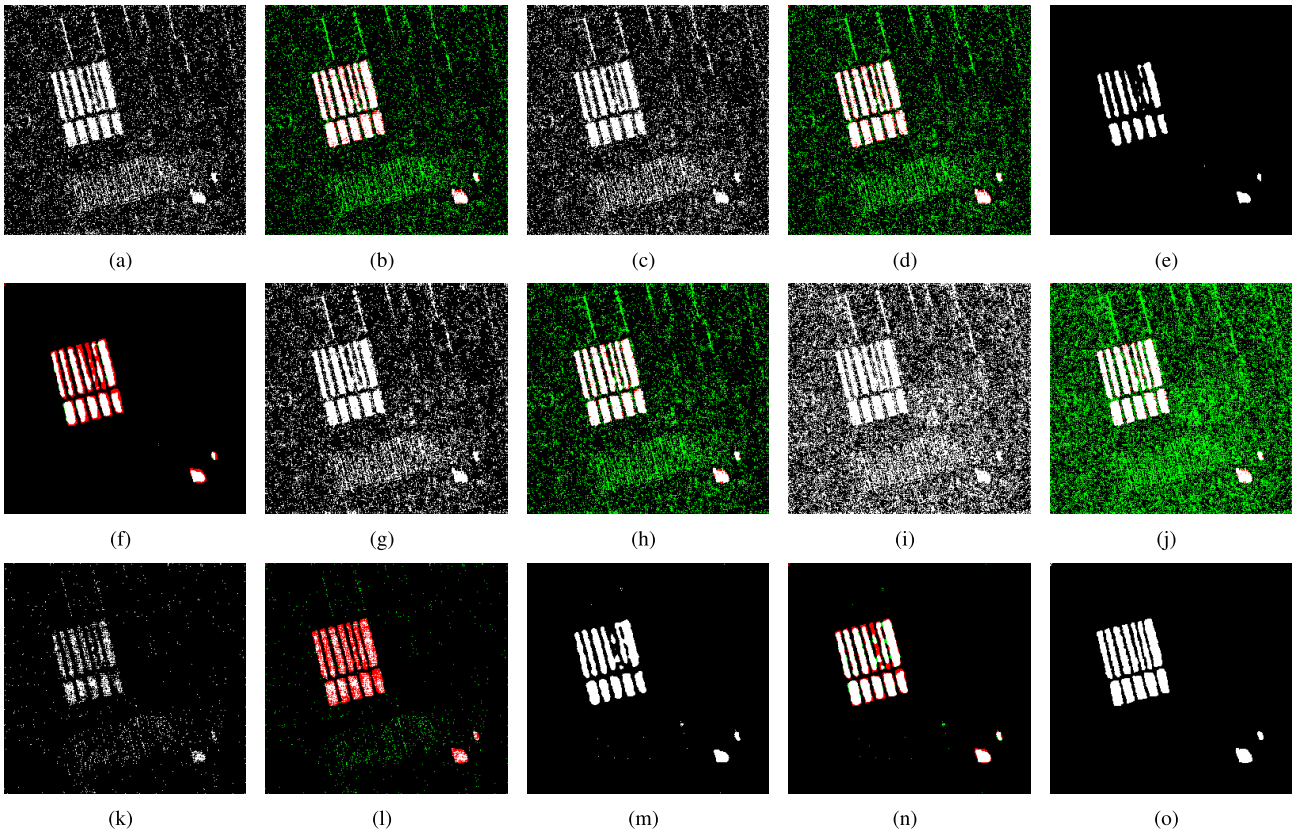

FIGURE 7. Change detection results about the farmland area of the Yellow River dataset obtained by (a) and (b): k-means, (c) and (d): FCM, (e) and (f): FLICM, (g) and (h): ICV, (i) and (j): FEBAC, (k) and (l): EMLS, (m) and (n): proposed MRFFAC, and (o): reference image.

TABLE 3. Comparison of CD results on the Coastline area of the yellow river dataset obtained through the seven algorithms.

Algorithm	FA	MA	TE	Kappa
k-means	27994	300	28294	0.0495
FCM	32111	257	32368	0.0435
FLICM	3	795	798	0.5782
ICV	32681	214	32895	0.0448
FEBAC	48523	167	48690	0.0260
EMLS	2593	929	3522	0.1801
MRFFAC	403	367	770	0.7151

TABLE 4. Comparison of CD results about the farmland area of the yellow river dataset obtained through the seven algorithms.

Algorithm	FA	MA	TE	Kappa
k-means	10860	870	11730	0.3735
FCM	13889	742	14631	0.3197
FLICM	73	2067	2140	0.7377
ICV	14151	575	14726	0.3271
FEBAC	30161	362	30523	0.1565
EMLS	997	3210	4207	0.4718
MRFFAC	196	1012	1208	0.8686

4) RESULT ON THE FARMLAND AREA OF THE YELLOW RIVER DATASET

In this experiment, the dataset is composed of of two SAR images (both with the size of 306×291) over Yellow River. Fig. 7 exhibits change maps obtained by the seven MTCD methods. it can be visually concluded that the change maps obtained by k-means, FCM, ICV, and FEBAC contain lots of noise since these maps have lots of green pixels. As a result, many unchanged areas are detected in mistake for changed ones. However, the change maps obtained by FLICM and ICV contains lots of red pixels, which denotes that some changed areas are not detected by the two methods. It can be obviously found that change maps acquired by the MRFFAC are better than those of other algorithms.

The CD experiment results acquired through the seven methods are reported in Table 4. As shown in Table 4, some vital regions having already changed fail being detected for FLICM and EMLS (showing up as a relatively higher MA). It can be found that the MA value obtained by MRFFAC is lower than that of FLICM although the FA value of the FLICM algorithm is 73. It can be obviously seen that the FLICM could obtain lower FA but the result with higher MA. Therefore, the proposed MRFFAC has the lowest total errors. In comparison with the results of other algorithms, the superiority of the proposed MRFFAC algorithm is clearly observed.

V. CONCLUSION

In consideration of the existence of speckle noise in SAR images, we introduce the log-ration operator to transform the multiplicative noise to the additive noise. For the purpose of

dealing with the complicated noise, the MRF theory has been incorporated into the fuzzy ACM for CD in multitemporal SAR images. In this paper, the proposed MRFFAC model measures the degree of attenuation of the neighbors with the Euclidean distance from the neighbour pixels to the central one. Then the neighboring information has been considered in MRFFAC to modify the pixelwise prior probability. The MRF-based energy function and the updating formula have been proposed to formulate the evolution of ACM. In the proposed approach, the initial membership matrix is acquired by the FCM algorithm. Then we establish the energy matrix, compute the pixelwise prior probability, and calculate the fuzzy membership during iterations.

Four datasets have been used in the SAR image CD experiments. The proposed approach has achieved the lowest total errors among seven CD algorithms. In the future, we hope to improve the proposed approach in performance and computational effort, and apply it to detect the change regions of remote sensing images acquired by different sensors.

REFERENCES

[1] R. J. Radke, S. Andra, O. Al-Kofahi, and B. Roysam, "Image change detection algorithms: A systematic survey," *IEEE Trans. Image Process.*, vol. 14, no. 3, pp. 294–307, Mar. 2005.

[2] Y. Zhong, A. Ma, Y.-S. Ong, Z. Zhu, and L. Zhang, "Computational intelligence in optical remote sensing image processing," *Appl. Soft Comput.*, vol. 64, pp. 75–93, Mar. 2018.

[3] L. Jiao, M. Gong, S. Wang, B. Hou, Z. Zheng, and Q. Wu, "Natural and remote sensing image segmentation using memetic computing," *IEEE Comput. Intell. Mag.*, vol. 5, no. 2, pp. 78–91, May 2010.

[4] J. Mardian, A. Berg, and B. Daneshfar, "Evaluating the temporal accuracy of grassland to cropland change detection using multitemporal image analysis," *Remote Sens. Environ.*, vol. 255, Mar. 2021, Art. no. 112292.

[5] Q. Guo, J. Zhang, and Y. Zhang, "Multitemporal hyperspectral images change detection based on joint unmixing and information coguidance strategy," *IEEE Trans. Geosci. Remote Sens.*, vol. 59, no. 11, pp. 9633–9645, Nov. 2021.

[6] X. Huang, L. Zhang, and T. Zhu, "Building change detection from multitemporal high-resolution remotely sensed images based on a morphological building index," *IEEE J. Sel. Topics Appl. Earth Observ. Remote Sens.*, vol. 7, no. 1, pp. 105–115, Jan. 2013.

[7] C. Wu, B. Du, and L. Zhang, "Slow feature analysis for change detection in multispectral imagery," *IEEE Trans. Geosci. Remote Sens.*, vol. 52, no. 5, pp. 2858–2874, May 2014.

[8] B. Hou, Q. Wei, Y. Zheng, and S. Wang, "Unsupervised change detection in SAR image based on gauss-log ratio image fusion and compressed projection," *IEEE J. Sel. Topics Appl. Earth Observ. Remote Sens.*, vol. 7, no. 8, pp. 3297–3317, Aug. 2014.

[9] F. Bujor, E. Trouve, L. Valet, J.-M. Nicolas, and J.-P. Rudant, "Application of log-cumulants to the detection of spatiotemporal discontinuities in multitemporal SAR images," *IEEE Trans. Geosci. Remote Sens.*, vol. 42, no. 10, pp. 2073–2084, Oct. 2004.

[10] N. Bova, O. Ibanez, and O. Cordon, "Image segmentation using extended topological active nets optimized by scatter search," *IEEE Comput. Intell. Mag.*, vol. 8, no. 1, pp. 16–32, Feb. 2013.

[11] Y. Bazi, L. Bruzzone, and F. Melgani, "An unsupervised approach based on the generalized Gaussian model to automatic change detection in multitemporal SAR images," *IEEE Trans. Geosci. Remote Sens.*, vol. 43, no. 4, pp. 874–887, Apr. 2005.

[12] E. H. Ruspini, J. C. Bezdek, and J. M. Keller, "Fuzzy clustering: A historical perspective," *IEEE Comput. Intell. Mag.*, vol. 14, no. 1, pp. 45–55, Feb. 2019.

[13] M. Gong, Z. Zhou, and J. Ma, "Change detection in synthetic aperture radar images based on image fusion and fuzzy clustering," *IEEE Trans. Image Process.*, vol. 21, no. 4, pp. 2141–2151, Apr. 2012.

[14] W. Fu, B. Xu, M. Zhang, and M. Johnston, "Fast unsupervised edge detection using genetic programming [application notes]," *IEEE Comput. Intell. Mag.*, vol. 13, no. 4, pp. 46–58, Nov. 2018.

[15] W. Yan, S. Shi, L. Pan, G. Zhang, and L. Wang, "Unsupervised change detection in SAR images based on frequency difference and a modified fuzzy *c*-means clustering," *Int. J. Remote Sens.*, vol. 39, no. 10, pp. 3055–3075, May 2018.

[16] X. Zhang, J. Chen, and H. Meng, "A novel SAR image change detection based on graph-cut and generalized Gaussian model," *IEEE Geosci. Remote Sens. Lett.*, vol. 10, no. 1, pp. 14–18, Jan. 2012.

[17] M. Gong, Y. Li, L. Jiao, M. Jia, and L. Su, "SAR change detection based on intensity and texture changes," *ISPRS J. Photogramm. Remote Sens.*, vol. 93, pp. 123–135, Jul. 2014.

[18] F. Chatelain, J.-Y. Tourneret, and J. Inglada, "Change detection in multisensor SAR images using bivariate gamma distributions," *IEEE Trans. Image Process.*, vol. 17, no. 3, pp. 249–258, Mar. 2008.

[19] G. Liu, L. Li, L. Jiao, Y. Dong, and X. Li, "Stacked Fisher autoencoder for SAR change detection," *Pattern Recognit.*, vol. 96, Dec. 2019, Art. no. 106971.

[20] S. Ahmadi and S. Homayouni, "A novel active contours model for environmental change detection from multitemporal synthetic aperture radar images," *Remote Sens.*, vol. 12, no. 11, p. 1746, May 2020.

[21] J. Chen, Q. Wang, J. Wang, and N. Li, "Change detection of water index in Danjiangkou reservoir using mixed log-normal distribution based active contour model," *IEEE Access*, vol. 7, pp. 95430–95442, 2019.

[22] M. Hao, W. Shi, H. Zhang, and C. Li, "Unsupervised change detection with expectation-maximization-based level set, *IEEE Geosci. Remote Sens. Lett.*, vol. 11, no. 1, pp. 210–214, Jan. 2013.

[23] X. Shan, X. Gong, Y. Ren, and A. K. Nandi, "Image segmentation using an active contour model based on the difference between local intensity averages and actual image intensities," *IEEE Access*, vol. 8, pp. 43200–43214, 2020.

[24] B. Han and Y. Wu, "Active contour model for inhomogenous image segmentation based on Jeffreys divergence," *Pattern Recogn.*, vol. 107, Nov. 2020, Art. no. 107520.

[25] C. Li, C.-Y. Kao, J. C. Gore, and Z. Ding, "Implicit active contours driven by local binary fitting energy," in *Proc. IEEE Conf. Comput. Vis. Pattern Recognit.*, Jun. 2007, pp. 1–7.

[26] S. Lankton and A. Tannenbaum, "Localizing region-based active contours," *IEEE Trans. Image Process.*, vol. 17, no. 11, pp. 2029–2039, Nov. 2008.

[27] B. Wang, X. Gao, D. Tao, and X. Li, "A unified tensor level set for image segmentation," *IEEE Trans. Syst., Man, Cybern., B, Cybern.*, vol. 40, no. 3, pp. 857–867, Jun. 2010.

[28] E. S. Brown, T. F. Chan, and X. Bresson, "Completely convex formulation of the Chan-Vese image segmentation model," *Int. J. Comput. Vis.*, vol. 98, no. 1, pp. 103–121, 2012.

[29] C. Darolti, A. Mertins, C. Bodensteiner, and U. G. Hofmann, "Local region descriptors for active contours evolution," *IEEE Trans. Image Process.*, vol. 17, no. 12, pp. 2275–2288, Dec. 2008.

[30] Y. Li, G. Cao, T. Wang, Q. Cui, and B. Wang, "A novel local region-based active contour model for image segmentation using Bayes theorem," *Inf. Sci.*, vol. 506, pp. 443–456, Jan. 2020.

[31] V. Caselles, R. Kimmel, and G. Sapiro, "Geodesic active contours," *Int. J. Comput. Vis.*, vol. 22, no. 1, pp. 67–79, 1997.

[32] D. Mumford and J. Shah, "Optimal approximations by piecewise smooth functions and associated variational problems," *Commun. Pure Appl. Math.*, vol. 42, no. 5, pp. 577–685, 1989.

[33] T. F. Chan and L. A. Vese, "Active contours without edges," *IEEE Trans. Image Process.*, vol. 10, no. 2, pp. 266–277, Feb. 2001.

[34] S. Osher and R. Fedkiw, *Level Set Methods and Dynamic Implicit Surfaces*. New York, NY, USA: Springer-Verlag, 2002.

[35] J. Gomes and O. Faugeras, "Reconciling distance functions and level sets," *J. Vis. Commun. Image Represent.*, vol. 11, no. 2, pp. 209–223, Jun. 2000.

[36] S. C. Zhu and A. Yuille, "Region competition: Unifying snakes, region growing, and Bayes/MDL for multiband image segmentation," *IEEE Trans. Pattern Anal. Mach. Intell.*, vol. 18, no. 9, pp. 884–900, 1996.

[37] D. Cremers, M. Rousson, and R. Deriche, "A review of statistical approaches to level set segmentation: Integrating color, texture, motion and shape," *Int. J. Comput. Vis.*, vol. 72, no. 2, pp. 195–215, Apr. 2007.

[38] I. Couso, C. Borgelt, E. Hullermeier, and R. Kruse, "Fuzzy sets in data analysis: From statistical foundations to machine learning," *IEEE Comput. Intell. Mag.*, vol. 14, no. 1, pp. 31–44, Feb. 2019.

[39] M. Gong, D. Tian, L. Su, and L. Jiao, "An efficient bi-convex fuzzy variational image segmentation method," *Inf. Sci.*, vol. 293, pp. 351–369, Feb. 2015.
[40] S. Krinidis and V. Chatzis, "Fuzzy energy-based active contours," *IEEE Trans. Image Process.*, vol. 18, no. 12, pp. 2747–2755, Dec. 2009.
[41] J. Fang, H. Liu, J. Liu, H. Zhou, L. Zhang, and H. Liu, "Fuzzy region-based active contour driven by global and local fitting energy for image segmentation," *Appl. Soft Comput.*, vol. 100, Mar. 2021, Art. no. 106982.
[42] J. Fang, H. Liu, L. Zhang, J. Liu, and H. Liu, "Region-edge-based active contours driven by hybrid and local fuzzy region-based energy for image segmentation," *Inf. Sci.*, vol. 546, pp. 397–419, Feb. 2021.
[43] A. Mondal, S. Ghosh, and A. Ghosh, "Robust global and local fuzzy energy based active contour for image segmentation," *Appl. Soft Comput.*, vol. 47, pp. 191–215, Oct. 2016.
[44] Y. Wu, W. Ma, M. Gong, H. Li, and L. Jiao, "Novel fuzzy active contour model with kernel metric for image segmentation," *Appl. Soft Comput.*, vol. 34, pp. 301–311, Sep. 2015.
[45] M. Gong, H. Li, X. Zhang, Q. Zhao, and B. Wang, "Nonparametric statistical active contour based on inclusion degree of fuzzy sets," *IEEE Trans. Fuzzy Syst.*, vol. 24, no. 5, pp. 1176–1192, Oct. 2015.
[46] R. Dekker, "Speckle filtering in satellite SAR change detection imagery," *Int. J. Remote Sens.*, vol. 19, no. 6, pp. 1133–1146, 1998.
[47] S. Krinidis and V. Chatzis, "A robust fuzzy local information C-means clustering algorithm," *IEEE Trans. Image Process.*, vol. 19, no. 5, pp. 1328–1337, May 2010.
[48] S. P. Chatzis and T. A. Varvarigou, "A fuzzy clustering approach toward hidden Markov random field models for enhanced spatially constrained image segmentation," *IEEE Trans. Fuzzy Syst.*, vol. 16, no. 5, pp. 1351–1361, Oct. 2008.
[49] T. X. Pham, P. Siarry, and H. Oulhadj, "Segmentation of MR brain images through hidden Markov random field and hybrid metaheuristic algorithm," *IEEE Trans. Image Process.*, vol. 29, pp. 6507–6522, 2020.
[50] H. Bi, L. Xu, X. Cao, Y. Xue, and Z. Xu, "Polarimetric SAR image semantic segmentation with 3D discrete wavelet transform and Markov random field," *IEEE Trans. Image Process.*, vol. 29, pp. 6601–6614, 2020.
[51] C. Zheng, Y. Zhang, and L. Wang, "Multigranularity multiclass-layer Markov random field model for semantic segmentation of remote sensing images," *IEEE Trans. Geosci. Remote Sens.*, vol. 59, no. 12, pp. 10555–10574, Dec. 2020.
[52] J. Sun and M. F. Tappen, "Learning non-local range Markov random field for image restoration," in *Proc. CVPR*, Jun. 2011, pp. 2745–2752.
[53] M. Li and T. Q. Nguyen, "Markov random field model-based edge-directed image interpolation," *IEEE Trans. Image Process.*, vol. 17, no. 7, pp. 1121–1128, Jul. 2008.
[54] C. D'Elia, G. Poggi, and G. Scarpa, "A tree-structured Markov random field model for Bayesian image segmentation," *IEEE Trans. Image Process.*, vol. 12, no. 10, pp. 1259–1273, Oct. 2003.
[55] M. Gong, L. Su, M. Jia, and W. Chen, "Fuzzy clustering with a modified MRF energy function for change detection in synthetic aperture radar images," *IEEE Trans. Fuzzy Syst.*, vol. 22, no. 1, pp. 98–109, Feb. 2013.
[56] W. Xiaoliang and L. Chunsheng, "Multiphase segmentation of SAR images with level set evolution," in *Proc. IEEE WRI Global Congr. Intell. Syst.*, vol. 2, May 2009, pp. 447–452.

FEI XIE (Member, IEEE) received the B.S. degree in computer science and technology from Xianyang Normal University, in 2007, the master's degree in software engineering from the University of Science and Technology of China, in 2009, and the Ph.D. degree in computer application technology from Northwest University.

He is currently a Researcher with the School of AOAIR, Xidian University, China. His main research interests include the theoretical research of image processing and pattern recognition and their application.

WENYUAN QIAO received the B.S. degree in telecommunication engineering from Xidian University, Xi'an, China, in 2011, where he is currently pursuing the Ph.D. degree in electronics science and technology with the School of Electronic Engineering. His research interests include deep neural networks, representation learning, and the application in remote sensing image processing.

TIANQI GAO was born in 1997. He received the B.Eng. degree from Xidian University, Xi'an, China, in 2019, where he is currently pursuing the Ph.D. degree in electronic science and technology with the Key Laboratory of Intelligent Perception and Image Understanding of Ministry of Education of China. His research interests include remote sensing image interpretation and computational intelligence.

QUN DUAN received the B.S. degree in computer science and technology from the Shaanxi University of Science and Technology, in 2002, and the master's degree in software engineering from East China Normal University. She is currently a Computer Teacher with Xianyang Normal University, China. Her main research interest includes image clarity processing.

TIANSHI LUO received the B.S. degree in electronic engineering from Xidian University, Xi'an, China, in 2021, where he is currently pursuing the Ph.D. degree in electronics science and technology with the School of Electronic Engineering. His research interests include deep neural networks, reinforcement learning, and multi-task learning.

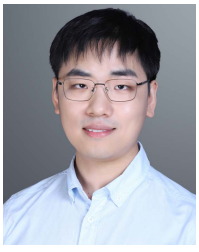

HAO LI (Member, IEEE) received the B.S. degree in electronic engineering and the Ph.D. degree in pattern recognition and intelligent systems from Xidian University, Xi'an, China, in 2013 and 2018, respectively.

He is currently an Associate Professor with the School of Electronic Engineering, Xidian University. His research interests include computational intelligence and machine learning. He served as a member for the Neural Networks Technical Committee. He received the Excellent Doctoral Dissertation Award of Shaanxi, in 2021.